Journal Name

Cite this: DOI: 10.1039/c0xx00000x

www.rsc.org/xxxxxx

ARTICLE TYPE

Interplay between the Structural and Magnetic Probes in Elucidation of the Structure of Novel 2D Layered $V_4O_4(OH)_2(O_2CC_6H_4CO_2)_4$·DMF

Igor Djerdj*[a,b], Srečo D. Škapin[c], Miran Čeh[c], Zvonko Jagličić[d,e], Damir Pajić[d,f], Bojan Kozlevčar[g], Bojan Orel[h], and Zorica Crnjak Orel[b]

Received (in XXX, XXX) Xth XXXXXXXXX 200X, Accepted Xth XXXXXXXXX 200X

First published on the web Xth XXXXXXXXX 200X

DOI: 10.1039/b000000x

The title compound has been synthesized under solvothermal conditions by reacting vanadium(V) oxytriisopropoxide with terephthalic acid in N,N-dimethylformamide. A combination of synchrotron powder diffraction, infrared spectroscopy, scanning and transmission electron microscopy, thermal and chemical analysis elucidated the chemical, structural and microstructural features of new 2D layered inorganic-organic framework. Due to the low-crystallinity of the final material, its crystal structure has been solved from synchrotron X-ray powder diffraction data using a direct space global optimization technique and subsequent constraint Rietveld refinement. [$V_4O_4(OH)_2(O_2CC_6H_4CO_2)_4$·DMF] crystallizes in the monoclinic system (space group P2/m (No. 10)); cell parameters: a = 20.923(4), b = 5.963(4), c = 20.425(1) Å, β = 123.70(6) °, V = 2120.1(9) Å^3, Z = 2. The overall structure can be described as an array of parallel 2D layers running along [-101] direction, consisting of two types of vanadium oxidation states and coordination polyhedra: face-shared trigonal prisms (V^{4+}) and distorted corner-shared square pyramids (V^{5+}). Both configurations form independent parallel chains oriented along the 2-fold symmetry crystallographic *b*-axis mutually interlinked with terephthalate ligands in a monodentate mode perpendicular to it. The morphology of the compound exhibits long nanofibers, with the growth direction along the layered [-101] axis. The magnetic susceptibility measurements show that the magnetic properties of $V_4O_4(OH)_2(O_2CC_6H_4CO_2)_4$·DMF can be described by a linear antiferromagnetic chain model, with the isotropic exchange interaction of J = −75 K between the nearest V^{4+} neighbours of S = 1/2.

1 Introduction

High application potentials of inorganic-organic hybrid materials either metal-organic framework or extended inorganic-organic hybrids attracts a great attention of researchers which can be noticed by an increased number of the corresponding research reports. Such open-framework hybrid materials exhibit a high structural diversity,[1, 2] plethora of morphologies, variety of physical[3, 4] and chemical properties[5] and consequently potential applications in the fields of photochemistry,[6] electromagnetism,[6] catalysis,[7] gas storage,[8] capture of volatile organic compounds,[9] and sorption.[10, 11] Thousands of reported inorganic-organic hybrid structures found in structural or citation databases slowly leads to the saturation in the restricted field of the pure synthesis and structural characterization of novel hybrids and tends to shift the research focus to the properties investigation and especially targeted application. When the inorganic skeleton comprises the transition metal, the framework exhibits in addition some other remarkable electronic properties of condensed transition metal compounds like antiferro-[12-14] and ferrimagnetism,[15, 16] metal-insulator transition, ferroelectricity,[17] and combined ionic/electrical conductivity.[18] Moreover, even attractive multiferroic metal-organic framework can be also designed.[19, 20] The choice of vanadium as a metal center can be regarded as a rather challenging one which often ends in complex systems or models and bunch of new findings. The reason for that is the fact that vanadium forms compounds having its oxidation state in the range from 2+ to 5+.[21] Very often in the resulting compound vanadium appears in the mixed valence state.[22] It also possess 3d electrons leading to the non-diamagnetic ground state (except 5+ oxidation state) and therefore showing various magnetic phenomena like spin-glass behaviour, antiferromagnetic correlations, or even charge ordering.[22] One dimensional antiferromagnetism having an origin in 1D structure has also been reported for the case of vanadium-based inorganic-organic hybrid material.[12] There are large quantity of research papers reporting the formation of inorganic-organic hybrid materials containing vanadium as a metal center,[23, 24] shared metal center or appearing as inorganic cluster. Organic linkers usually employed in the synthesis of vanadium-based inorganic-organic hybrids yielded to the formation of terephthalate,[25] isophthalate,[26] polyoxometalate,[27, 28] pyromellitate,[29] phosphonoacetate,[30] oxobenzoate,[12] etc...

It is well-known that multifunctional organic molecules with one or more carboxylic acid groups are rigid and able to coordinate to several metal centers in various modes,[31] and therefore are widely implemented in the design of inorganic-organic hybrid materials, which was documented by the large number of reported compounds. For instance, the usage of biphenyl-4,4'-dicarboxylic acid, and Co/Zn as a metal center yielded to formation of Co/Zn-bpdc coordination polymer,[32, 33] porous chromium terephthalate (MIL-101) has been formed under microwave radiation,[34] several metal-organic frameworks have been constructed with flexible aromatic dicarboxylate ligands and N-donor ligands,[35] vanadium oxyterephthalate (MIL-47) with very large pores and high magnetic characteristics has been hydrothermally synthesized,[25] vanadocarboxylate (MIL-68) has been synthesized in a non-aqueous medium[36] and many other complexes containing one or more carboxylic acid groups as participating ligand molecules.[31, 37-41]

Major reported inorganic-organic hybrid structures have been prepared using single crystal growth in aqueous medium. However, there is still enough space in the field by implementing synthetic protocol based on the non-aqueous sol-gel routes. Such approach has

been promoted as a valuable alternative to aqueous synthetic pathways. Nonaqueous sol-gel synthesis gave access to a large variety of metal oxide nanoparticles,[42-44] oxide-based inorganic-organic hybrids,[45, 46] metal (oxide) hydroxides,[22, 47] and doped metal oxides.[48, 49]

Herein, we present the continuation of our previously published research of vanadium-based inorganic-organic hybrids,[12] extended this time to new hybrid compound prepared using dicarboxylic organic linker i.e. terephthalic acid. The motivation for such a choice was the well-known hydrothermally synthesized MIL-47 compound[25], having a similar chemical composition and constitutive fragments as our obtained compound. However, in the following lines it will be shown that our solvothermal approach yields to very different findings in terms of structure, composition, thermal and magnetic properties than as reported for MIL-47 compound.

2 Experimental

2.1 Synthesis

All procedures were started in a glovebox (O_2 and H_2O < 0.1 ppm). In a typical synthesis of nanofibers, 0.6 mmol o vanadium (V) triisopropoxide and 0.9 mmol of terephthalic acid (98%; Aldrich) were added to 20 mL of anhydrous N,N-dimethylformamide (DMF) (99.8%; Aldrich). The reaction mixture was transferred into the autoclave (VACUTECH, Ljubljana, with a Teflon cup of 45 ml inner volume). The autoclave was taken out of the glovebox and heated at 180 °C for 72 hours. The resulting suspension was centrifuged, and the precipitate was thoroughly washed 3 times with ethanol and dried in a oven at 60 °C for several hours until the dried stable dark yellow powder was obtained.

2.2 Characterization

The as prepared solid was pre-analyzed in the reflection mode (CuKα radiation) by X-ray powder diffraction (XRD) using D4 Endeavor Bruker AXS in an angular range 2θ from 3 to 70 degrees with a step size of 0.02° and a collection time of 3 seconds. However, for the structural solving and refinement, a laboratory XRD was not enough, since for such a job the best possible XRD pattern is a must. Therefore, a high-resolution X-ray powder diffraction pattern has been collected from the synchrotron radiation source at the powder diffraction station of Swiss-Norwegian beam line at the European Synchrotron Radiation Facility in Grenoble. A glass capillary of 0.8 mm in diameter was oscillated by 60° during exposure to the X-ray beam for 60 s, followed by readout for ~83 s. The measurement has been performed at room temperature. The data were collected using a MAR345 image plate detector at a sample to detector distance of 250 or 400 mm and radiation with wavelength λ = 0.70177 Å.

The morphology and a particle size were examined by using a scanning electron microscope FE-SEM SUPRA 35VP (Carl Zeiss) equipped with an energy-dispersive spectrometer (EDXS, Inca 400, Oxford Instruments).

The TEM observations were carried out in a transmission electron microscope operated at 200 kV (Model JEM-2100, JEOL, Japan) which is equipped with an X-ray spectrometer for energy-dispersive X-ray spectroscopy (EDXS). TEM samples were prepared by dispersing the powders in ethanol using an ultrasonification followed by the deposition of the obtained suspension on carbon-coated copper grids.

The chemical composition was determined based on the results of the elemental analysis. CHN elemental analysis was performed with a Perkin-Elmer 2400 CHN Elemental Analyzer. Vanadium content was determined using an inductively coupled plasma atomic emission spectrometry (ICP-AES) employing an Atomscan 25, Thermo-Jarrell Ash (USA) sequential instrument. Fourier transform infrared spectra (FTIR) were obtained with a rapid FTIR spectrometer (FTS 6000). Before each measurement, the background spectrum was taken and subtracted from the FTIR spectrum of the sample. Thermal stability of the material was probed by the thermogravimetric analysis (TGA) which was performed on Netzsch TG 209 F1 at a scanning rate of 20 °C/min under an air atmosphere.

Bulk DC magnetic properties have been studied with a QUANTUM DESIGN MPMS-XL-5 SQUID magnetometer. Zero-field and field-cooled runs were performed between room temperature and 2 K in a static magnetic field of 1000 Oe. For the magnetization measurements samples were loaded into gelatine capsule and the measurements were corrected for the diamagnetic contribution of the sample holder.

2.3 Structure solution and refinement

The observed first 15 reflections of $V_4O_4(OH)_2(O_2CC_6H_4CO_2)_4 \cdot DMF$ were indexed with the auto-indexing program WDICVOL04.[50] The solution with figure of merit [M(15) = 19, F(15) = 71(0.003117, 68)] has been chosen between monoclinic solutions which indexed all selected peaks. A monoclinic cell was found (a = 20.923(4), b = 5.963(4), c = 20.425(1) Å, β = 123.70(3) º) with no other observable systematic extinctions. The structure has been solved in the space group $P2/m$ (10) using the program FOX[51] and the direct space method. Based on the refined unit cell volume (2120.3(9) Å^3), and the generally accepted rule that the volume per non-hydrogen atom should be between 15 and 20 Å^3, the number of chemical formula units per unit cell Z = 2. In accordance with that at the beginning of FOX optimization the structure has been modelled with two rigid restrained VO conditionally stated molecules and two independent rigid terephthalate molecules $O_2CC_6H_4CO_2$ kept in a flat conformation. The initial assumption of the optimization was that all optimized objects reside in general position having site multiplicity 4. However, in the course of the optimization, vanadium atoms tended to occupy special positions with the multiplicity 2, and accordingly two more VO molecules have been included in the optimization. The final solution comprised 2 terephthalate molecules in general positions (4o) and 4 vanadium atoms in special positions each (2×2m, and 2×2n). The same correct solution was identified in several global optimization runs of around one hour each.

The optimized structural model was further refined with the Rietveld method by using the program FULLPROF.[52] The crucial point in this constrained refinement was the proper restrain of V−O bonds and O−V−O angles defining coordination polyhedra around vanadium. Previously direct space optimized model together with the magnetic measurement results indicated the presence of the mixed valence state of vanadium V^{4+} and V^{5+}, and accordingly the structure comprised two different vanadium coordination polyhedra: trigonal prism (coordination number 6) which surrounds V^{4+} and square pyramid (coordination number 5) around V^{5+}. The former has been

modelled by restraining all six V−O distances to 1.9 Å, where four of them belong to vanadium coordinating oxygens of two different terephthalate molecules while two remaining oxygens (one independent site O25) directly bridges neighbouring vanadium sites. The square pyramid has been obtained by imposing three V−O distances to 1.7 Å (1 vanadium coordinating oxygen which belong to non-bonding apex carrying OH group and 2 direct bridging oxygens O30), while the remaining two oxygens originating from terephthalate molecules were restrained to 2.0 Å. The terephthalate molecules were described as semi-rigid bodies using the internal coordinates (Z-matrix). The phenyl ring of both terephthalate molecules was kept flat by fixing atomic coordinates of carbon atoms, i.e. during the Rietveld refinement they are kept constant with the values obtained in the FOX optimization. Varying of the oxygen atom coordinates was done by constraining C−O distances within the limit of 1.33 Å. The DMF molecule has been placed at the intersection of (-202) plane and unit cell by approximate positioning of nitrogen atom in the middle between (-101) layers. The whole molecule has been refined by restraining C−N and C−O distances and O−C−N angle according to the molecular geometry. In order to fulfil compositional requirement for 2 DMF molecules per unit cell, the constitutive atoms are regarded planar lying in *ac* plane on special positions 2m. The diffraction profiles were described by the Thompson-Cox-Hastings pseudo-Voigt, and the background by linear interpolation of a set background points with refinable heights. The observed anisotropic line broadening was supposed to be due to the anisotropic crystallite size, and was described by a needle-like coherent domains model. Four isotropic displacement parameters (vanadium, carbon, nitrogen and oxygen atoms) were refined. In the final run 48 structural, 4 lattice parameters, 8 profile and 52 background parameters were allowed to vary. The hydrogen atoms were finally attached to the corresponding C and O atoms using the program OLEX 2.[53]

3 Results and discussion

3.1 Crystal structure description

The thoroughly washed and dried as synthesized compound appears as a dark yellow powder. The extraction of chemical formula of as prepared compound was not straightforward, due to the presence of more than one oxidation state of vanadium in the final compound V^{5+}, and V^{4+}. Such information has been obtained from the preliminary DC magnetic susceptibility measurement which will be shown in more details below. Nevertheless, by combining the results of CHN, ICP-AES analysis and magnetic susceptibility results the proposed formula is: $V_4O_4(OH)_2(O_2CC_6H_4CO_2)_4\cdot$DMF; elemental analysis calcd. (%): C 40.76, H 2.44, N 1.36, V 19.76; found: C 40.29, H 2.60, N 1.37, V 19.40. The main assumption in the deduction of such chemical formula was the presence of V^{5+} and V^{4+} oxidation states in equal proportions (1:1), although the preliminary magnetic results indicates even higher quantity of V^{5+}. However, the major domination of 5+ oxidation state in the single phase would be impossible to establish within the structure due to the lack of interacting neighbouring spins (only V^{4+} can magnetically interact) which contradicts to the detected non-diamagnetic ground state.

The crystal structure of the title compound has been solved and refined from the synchrotron powder XRD pattern. Figure 1 shows a typical Rietveld output plot of the synchrotron powder X-ray diffractogram of $V_4O_4(OH)_2(O_2CC_6H_4CO_2)_4\cdot$DMF recorded at T = 293 K. The agreement factors are as follows: R_{wp} (not corrected for background) = 9.74%, R_{wp} (corrected for background) = 15.1%, χ^2 = 3.08, R_{Bragg} [$V_4O_4(OH)_2(O_2CC_6H_4CO_2)_4\cdot$DMF] = 5.52%. Taking into account that the number of independent contributing reflections in the refinement interval is extremely high and amounts to 816 causing an overlap between adjacent reflections which implies uncertainty in the profile fitting, furthermore an asymmetric unit is rather large (comprising 37 non-H atoms) with a high number of restraints imposed in the refinement of the final structural model, one can state based on the values of aforementioned agreement factors that the $V_4O_4(OH)_2(O_2CC_6H_4CO_2)_4\cdot$DMF refines very well. Slightly larger value of χ^2 indicates the presence of minor secondary phase or even phases not described by the structural model. Careful inspection of the Rietveld plot shows that some peaks (2θ = 7.01, 7.64, and 8.81°) are not fully explained by the structural model. It can be attributed to impurities of an unknown phase produced as a byproduct during the synthesis. The corresponding final crystallographic parameters including refinement details are summarized in Table 1, refined structural parameters in Table S1 in Supplementary Information, and selected interatomic distances and angles in Table 2. A major feature of the structure is a two-dimensional network of two types of vanadium polyhedra: face-shared trigonal prisms and distorted corner-shared square pyramids (Figures 2(a)-(d)). Both configurations form independent parallel chains oriented along the 2-fold symmetry crystallographic *b*-axis mutually interlinked with terephthalate ligand perpendicular to it along the [-101] direction. Adjacent two-dimensional layers are mutually further stabilized by hydrogen mediated weak interaction which is achieved in two modes: Two 2-fold rotational- symmetry related layers, depicted in the projection as a central column in Figure 2(d), are stabilized via C–H···O hydrogen contacts with lengths of 2.25 and 2.93 Å. Between the parallel layers from the adjacent unit cells (Figure 2 (b)) a void is present, in which two N,N-dimethylformamide molecules are accommodated. Their incorporation participates in the cohesion of the structure with the mentioned hydrogen contacts C–H···O between layers, with distances of 2.19 Å linking DMF and the central layer, and 1.80 Å between DMF and the layer intersecting unit cell vertices shown in Figure 2(b).

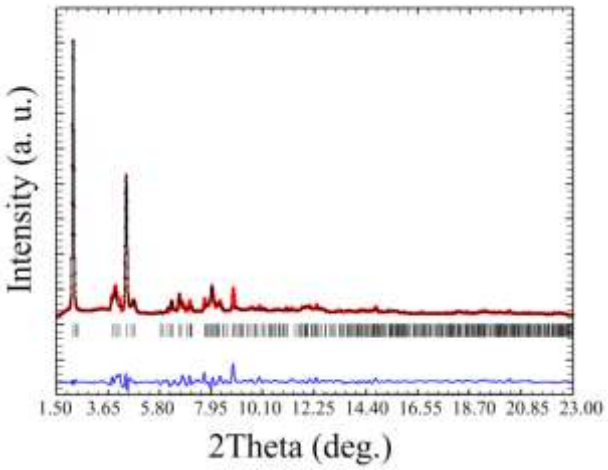

Fig. 1 Rietveld output plot of $V_4O_4(OH)_2(O_2CC_6H_4CO_2)_4 \cdot DMF$. Observed (red), calculated (black) intensities and their difference curve (blue) are denoted. In addition, calculated Bragg positions of the $V_4O_4(OH)_2(O_2CC_6H_4CO_2)_4 \cdot DMF$ are indicated by vertical ticks.

Table 1. Crystallographic data and refinement parameters obtained from synchrotron X-ray powder diffraction pattern.

chemical formula	$V_4O_4(OH)_2(O_2CC_6H_4CO_2)_4 \cdot DMF$
empirical formula	$V_4H_{25}C_{35}N_1O_{23}$
V-oxidation number(s)	+4 (50%), +5 (50%)
space group	*P*2/m (10)
molecular weight	1031.33
Z	2
crystal system	monoclinic
lattice parameters (Å)	*a* = 20.923(4)
	b = 5.963(4)
	c = 20.425(3)
	β = 123.701(6) º
cell volume (Å^3)	2120.1(15)
calculated density (g/cm^3)	1.613(1)
data collection range	1.5 to 23.5 º
restricted data analysis range	1.5 to 23.5 º
wavelength (Å)	0.70177
no. of contributing reflections	816
no. of parameters refined	112
no. of bond lengths restrained	47
no. of bond angles restrained	42
average apparent crystallite size (nm)	31.4
standard deviation of the size -measure of anisotropy (nm)	41.8
R_p (background corr.), R_{wp}, R_{exp}, R_B (%)	12.3, 15.1, 8.63
	5.52
χ^2	3.08

Vanadium atoms occupy four different crystallographic sites denoted in Table S1 as V1-V4. However, V1 and V2, and separately V3 and V4 are equivalent from the point of view of the coordination environment. Coordination of V1 (V2), where vanadium atom is in oxidation state 4+, has an almost regular trigonal prismatic geometry (Figure S1 in Supplementary Information) with four terephthalate ligands, each shared between two adjacent vanadium atoms, while two remaining structural oxygens are directly bonded to vanadium making V–O–V–O... bonds along *b*-axis. The vanadium to oxygen distances are almost identical ranging from 1.89 to 1.963 Å. Such shared coordination of four terephthalate ligands (4×0.5, 0.5 is an effective charge of ligand) and two shared structural oxygen anions (2×1) around V1 and V2 are necessary for V^{4+} charge balance. According to our model deduced from the magnetic susceptibility measurements, remaining vanadium sites V3 (V4) have atoms in oxidation state +5. Charge balance in this case has been accomplished with the coordination number 5 i.e. distorted square pyramid as depicted in Figure 2(a) and Figure S2 in Supplementary Information. Vanadium atom is surrounded by two oxygen atoms being part of two mirror-symmetric terephthalate ligands, two bridging structural oxygens, and one single bonding OH group (H is attached to O11 in Figure S2). Four oxygen atoms lie in the basal plane of VO_5 square pyramid at distances of 1.62 and 2.08 Å, while an apical OH group is located at the distance of 1.85 Å. One should note that the shortest V–O bond is not the apical one as one might expect, but the equatorial bond connecting vanadium with bridging oxygen (V3–O10, V4–O10). It implies that the strongest interaction occurs between vanadium and bridging oxygen in this coordination. An apical angle(s), measured as an angle(s) between an apical bond and equatorial bonds, in our case amounts to 103.8, and 105.3° for V3 (Table 2), while for V4 case the pyramidal distortion is slightly larger since two apical angles differ larger from each other (89.7, and 105.1°). In stable square pyramidal structures the apical angle is usually found between 100 and 106°, confirming our results.[54] The most important part of

the proposed structural models in inorganic-organic hybrids in general is coordination geometry around the metal center. The calculated electronic structure usually deduced from DFT highly reflects the coordination geometry and furthermore influences the measured physical properties and phenomena. As a matter of fact, it is very important to ensure about the correctness of the proposed structural model. One way to do this is to estimate the oxidation state of the V ions in the structure by calculating the well-known bond-valence sum rule.[55] Calculating the bond-valence sum (BVS) for vanadium atom V^{+4} in the VO_6 trigonal prismatic coordination, one obtains the value of BVS of 4.15 for V1, and 4.13 for V2. In the case of V^{+5} square pyramidal coordination, obtained BVS values are 5.11 for V3 and 5.74 for V4. By comparison with the formal oxidation states of all vanadium atoms from the asymmetric unit, all calculated BVS values agree well with them (a slight deviation is found for V4), confirming the validity of the proposed structural model. Besides four vanadium atoms, two independent direct-bonded V–O–V oxygens, two independent OH groups, and two DMF molecules, an asymmetric unit contains two crystallographically independent terephthalate ligands which act in the same fashion. Both carboxylates of these two independent terephthalate moieties coordinate to vanadium center in a monodentate mode. The remaining non-bonding oxygen from carboxylates is in a weak interaction with hydrogen from the phenyl ring in an adjacent layer, while the oxygen from another carboxylate group of the same terephthalate moiety is again in the hydrogen contact to DMF molecule, as nicely visible in Figure 2(b).

Table 2. Selected bond lengths (Å) and angles (deg) with esds in parentheses.

Atoms	Distance (Å)	Atoms	Angle (deg)
V1-O1 (2×)	1.92(2)	O1-V2-O5	76.5(4)
V1-O5 (2×)	1.954(8)	O1-V2-O1	98.9(3)
V1-O9 (2×)	1.89(1)	O1-V2-O9	59.2(3)
V2-O1 (2×)	1.92(2)	O9-O5-O1	50.2(9)
V2-O5 (2×)	1.963(7)	O5-O1-O9	50.7(9)
V2-O9 (2×)	1.89(1)	O1-O9-O5	79.1(8)
V3-O7 (2×)	2.08(4)	O7-V3-O10	81.9(9)
V3-O10 (2×)	1.62(5)	O7-V3-O7	52.6(8)
V3-(OH)11 (1×)	1.85(2)	O10-V3-O10	126.2(8)
V4-O10 (2×)	1.62(4)	(OH)11-V3-O7	103.8(9)
V4-O4 (2×)	2.00(3)	(OH)11-V3-O10	105.3(8)
V4-(OH)12 (1×)	1.70(8)	O4-V4-O10	68.4(9)
O8-H6	2.25(8)	O4-V4-O4	65.6(8)
O2-H15	2.93(7)	O10-V4-O10	143.6(9)
O3-H2b	2.19(6)	(OH)12-V4-O4	89.7(9)
O6-H3b	1.80(6)	(OH)12-V4-O10	105.1(9)

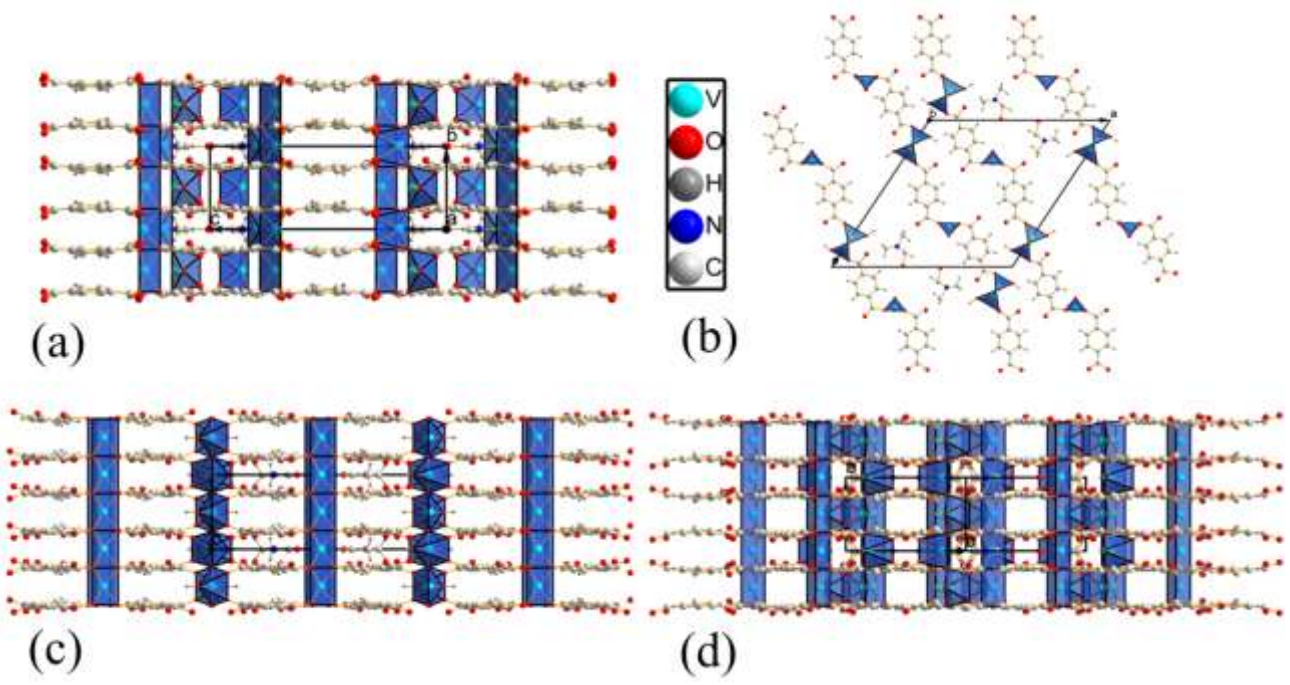

Fig. 2 Solved and refined final crystal structure of $V_4O_4(OH)_2(O_2CC_6H_4CO_2)_4 \cdot DMF$ viewed (a) along the *a*-axis, (b) along the *b*-axis, (c) along the *c*-axis, and (d) along the [-101] direction. Projection of the unit cell is indicated by solid lines.

The thermal behaviour of the obtained compound was studied by thermal analysis including thermogravimetric analysis (TGA) and differential thermal analysis (DTA). These combined experiments showed that as synthesized compound undergoes a single decomposition as evidenced from the single exothermic DTA peak centred at 428 °C as shown in Figure 3(a). This is the temperature where the degradation of the hybrid upon heating completes due to the ending of the combustion of the organic moiety. The absence of additional peaks in DTA curve at lower temperatures resolved some doubts originated from an elemental analysis about the possible incorporation of the crystalline water. Such incorporation would imply more than one step decomposition in TGA and extra peaks in DTA at the temperatures close to water boiling point would appear. Their absence revealed that the water is not involved in any form in the final compound and the excess of hydrogen atoms shown by an elemental analysis is then attributed to the structural OH groups. Assuming that the final product of decomposition is the most stable vanadium oxide V_2O_5, the observed net weight loss (65.1%) is consistent with the expected one (64.7%) based on the proposed empirical formula. Accordingly, TGA and DTA results also corroborate the proposed chemical formula of the investigated hybrid.

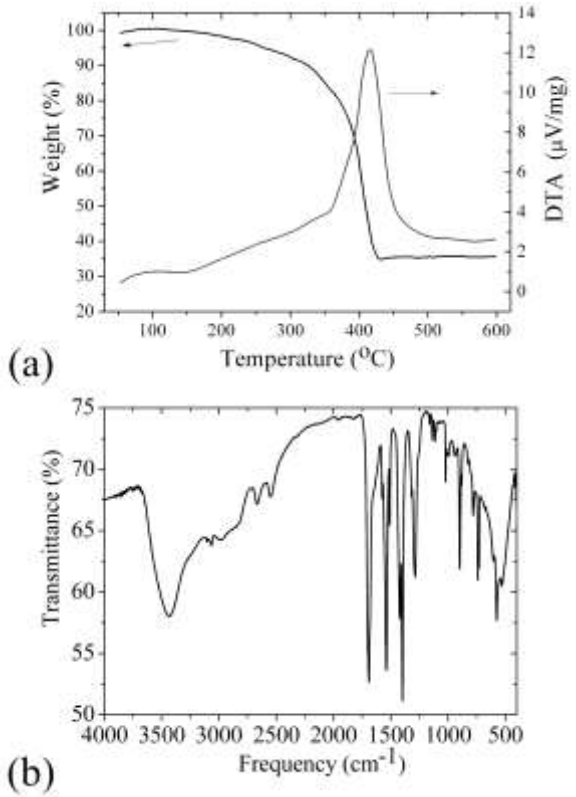

Fig. 3 (a) Thermal behaviour of $V_4O_4(OH)_2(O_2CC_6H_4CO_2)_4 \cdot DMF$, TGA, and DTA curves showing weight loss and thermal exchanges upon heating. (b) FT-IR spectrum of $V_4O_4(OH)_2(O_2CC_6H_4CO_2)_4 \cdot DMF$.

To find out more information about the organic moieties and their binding to the vanadium centers, the investigated compound has been analyzed by FT-IR spectroscopy. The resulting spectrum which is displayed in Figure 3(b) consists of a bunch of absorption peaks reflecting a high structural complexity of this hybrid compound. The spectrum itself can be split in two parts: Characteristic bands corresponding to the different molecular vibrations of the terephthalate ligand, and the bands attributed to vibrations of the inorganic O–V–O prismatic and/or pyramidal framework. The broad band centered at 3435 cm^{-1} is attributed to O−H stretching modes of the hydroxyl groups of adsorbed water molecules and hydrogen-bonded OH groups. When OH group is not involved in hydrogen bonding, its absorption band tends to be sharp. Based on the proposed composition of this compound with bonded OH groups to metal centers, it is expected the presence of such a sharp band. However, due to the highly surface adsorbed water it is difficult to resolve it in IR spectrum. It is interesting to note that the bands at 939 and 1287 cm^{-1}, characteristic of the dimeric structure of terephthalic acid (-COOH dimer), are still observed, pointing to the fact that a small amount of terephthalic acid dimers are also present in the sample.

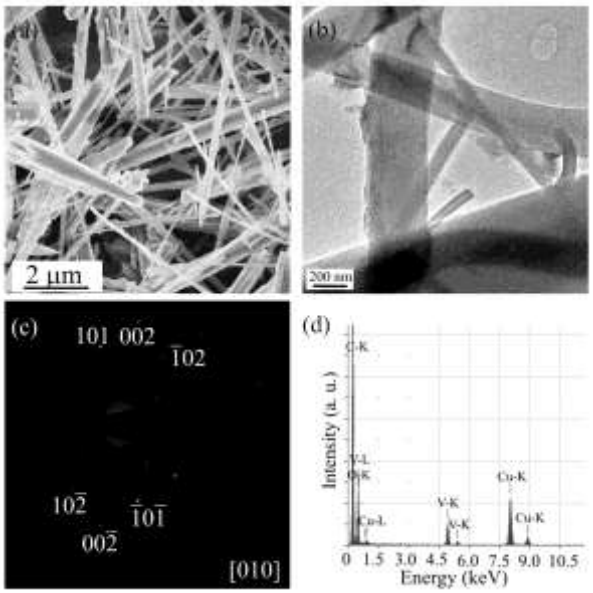

Fig. 4 (a) Overview SEM image of the as-synthesized $V_4O_4(OH)_2(O_2CC_6H_4CO_2)_4 \cdot DMF$ nanofibers. (b) TEM image recorded at a higher magnification. (c) Indexed SAED pattern of the single nanofiber in [010] zone-axis. (d) EDX spectrum recorded from the part of the nanofiber shown in (b). Cu originates from TEM grid.

The bands at 1576, 1539, 1509, and 1420 cm^{-1} are characteristic of the skeletal vibrations of the phenyl ring, the bands at 3105 and 3064 cm^{-1} can be assigned to stretching of sp^2 hybridized C−H bonds of the phenyl ring, while the band at 1162 cm^{-1} is typical of C−C vibration.[45, 56, 57] In the low-frequency range of 900-730 cm^{-1} another set of characteristic frequencies of the phenyl ring are observed, specifically the band at 730 cm^{-1} corresponds to the C−H out of plane deformation and the bands at 896, 782, and 739 cm^{-1} are assigned to the C−H bending vibrations.[57] Important information about the binding of the organic moieties, particularly the carboxylate anions, COO^-, to the metal centers, can be deduced by comparing the difference of frequencies between its antisymmetric ν_a and symmetric ν_s stretching modes. In the IR spectrum $\nu_a(COO^-)$ is located at 1692 cm^{-1} and $\nu_s(COO^-)$ at 1397 cm^{-1} leading to a frequency difference of Δ = 295 cm^{-1}. Monodentate coordination leads to a higher difference between asymmetric and symmetric carboxylate frequencies compared to bidentate ones (bridging, chelating). The strict border between monodentate and bidentate coordinations in terms of frequency difference has not been established, it depends on many parameters which describe particular chemical system including a metal type, a functional group type, etc...; it is a feature of a particular studied system. What we can do in our case is to compare this inorganic-organic system with the similar one previously reported, $VO(C_6H_5COO)_2$,[12] in which a frequency difference of Δ = 177 cm^{-1} has been found classifying that compound to bidentate bridging type that was also confirmed with DFT geometry optimization. Significantly larger Δ found in the case of $V_4O_4(OH)_2(O_2CC_6H_4CO_2)_4 \cdot DMF$, indicates to a monodentate coordination as suggested by the structural model extracted from the powder XRD pattern. The presence of N,N-dimethylformamide molecule in the examined compound can be also detected with FT-IR spectroscopy. The strongest band in the IR spectrum of DMF is characteristic of C=O stretching and can be found at around 1675 cm^{-1}. The strong observed band located at 1692 cm^{-1} which is previously assigned to antisymmetric stretching of carboxylate anion can be also identified as this DMF characteristic frequency, i.e. there is an overlap between DMF and COO^- characteristic vibrations.

The microstructural properties of the investigated compound, including morphology and the local crystallinity, have been probed by the electron microscopy including TEM, selected area electron diffraction (SAED) and SEM. A representative SEM overview image of $V_4O_4(OH)_2(O_2CC_6H_4CO_2)_4 \cdot DMF$ is displayed in Figure 4(a), from which it seems that the entire material is rather homogeneous in terms of shape, but inhomogeneous in terms of size, consisting of long nanofibers up to 10 μm in length and even up to several hundred nm in diameter. Moreover, a higher magnification TEM image (Figure 4(b)) clearly discloses that the nanofiber diameter distribution is not uniform, revealing the presence of individual nanofibers with diameters from 60 to 400 nm. The local crystallinity of the individual nanofiber has been tested by recording the corresponding electron diffraction pattern, taken from a selected region of a single nanofiber. The resulting pattern is displayed in Figure 4(c), showing that it consists of discrete Laue spots, thus revealing the single-crystallinity of the part of the investigated individual nanofiber. In addition, the symmetry of the Laue spots and the corresponding reflection assignment make it possible to identify a zone-axis as [010] (*b*-axis). To be sure that the imaged object really belongs to the desired hybrid compound, and not to the some sort of impurity of inorganic or organic origin, EDX microanalysis has been additionally performed and the resulting spectrum recorded from the same region as SAED is shown in Figure 4(d). The K-lines of vanadium are clearly resolved pointing that the observed crystalline material is targeted compound. In addition, the K-lines of C and O are evidenced as well, but the spectral signature of N is missing, since its fraction in the compound is close to the detecting limit of EXD spectrometer.

Based on the structural description given so far, one could wonder about the usage of prefix *nano* in the employed terminology in this research, due to the reported morphological sizes lying in the microsized region. The explanation why do we insist on term *nano*-fiber follows from basically two features: As obtained crystals were not big enough for single-crystal diffractometry, and secondly by analyzing XRD powder pattern, a non-negligible peak broadening occurs leading to the conclusion that the crystalline fibers are in nanoregime. It is generally expected in a system of reduced dimensionality that anisotropic broadening occurs, *i.e.*, crystallite sizes might

show a strong anisotropic character.[22] As described in the experimental part in more details, the anisotropic size broadening is considered by anisotropic modelling of those peaks in XRD pattern which do not fit well according to the proposed structural model and profile function details. The resulting highest value of the crystallite size 311.3 nm corresponds to the -101 reflection which is the preferred growth direction of the nanofibers. This feature is in accordance with the proposed structural model of parallel 2-dimensional layers arranged along the [-101] axis (Figure 2(d)). Overall average crystallite size amounts to 31.4 nm with high standard deviation as a measure of anisotropy (41.8 nm) confirming our assumed nanosized microstructural model.

3.2 Magnetic properties

The temperature dependence of the molar susceptibility $\chi(T)$ displayed in Figure 5 is obviously not pure paramagnetic (i.e. not $1/T$ dependence). The observed decrease of the product $\chi T(T)$ with decreasing temperature (inset to Figure 5) is an indication of the considerable antiferromagnetic coupling in the system. On the other hand, the susceptibility $\chi(T)$ continuously increases with decreasing the temperature, which may be attributed to the non-interacting paramagnetic magnetic moments in the structure. However, a small value of the susceptibility at the lowest temperature points to the small content of paramagnetic centers that could be regarded as paramagnetic impurities. Therefore, the product $\chi T(T)$ is here more suitable for quantitative analysis than $\chi(T)$, as $\chi T(T)$ emphasizes the antiferromagnetism presence. The structure of the complex suggests the arrangement of the magnetic moments on vanadium ions in chains. In accordance with that we tried to model the measured magnetic susceptibility with rationale function from the reference 58[58] that fits to the Bonner-Fisher curve[59] describing the susceptibility of a linear magnetic chains of spins S = 1/2 (vanadium(IV)) with the isotropic interaction between nearest neighbours given by $H = -2J\sum S_i \cdot S_j$. We add a Curie term for spin S = 1/2 to the function from 58[58] to account for the non-interacting paramagnetic moments, and the temperature constant term χ_0 due to the diamagnetic contribution of the inner core electrons and the temperature independent paramagnetism. The final formula used for fitting to the experimental data in form of $\chi T(T)$ is:

$$\chi = A\frac{N_A g^2 \mu_B{}^2}{k_B T}\frac{0.25+0.14995x+0.30094x^2}{1.0+1.9862x+0.68854x^2+6.0626x^3}+B\frac{N_A g^2 \mu_B{}^2}{4k_B T}+\chi_0, \qquad (1)$$

g = 2.0 is used for g-factor, N_A is the Avogadro number, μ_B Bohr magneton, k_B Boltzmann constant and $x = |J|/T$ where the interaction J (in Kelvins) is negative for antiferromagnetically coupled magnetic moments. Coefficients A and B are atomic fractions of vanadium(IV) magnetic moments with S=1/2 in chains and non-interacting vanadium(IV), respectively.

Fitting of the function (1) to the measured data was performed in a way consistent with the solved structure. Namely, the constraint $A + B = 0.5$ is taken because the A and B parameters refer to V^{4+} ions that occupy half of vanadium sites and the other half are V^{5+} ions. The result is $A = 0.462$, $B = 0.038$, $J = -75$ K, $\chi_0 = 3.5\cdot10^{-4}$ emu/mol. The constant term χ_0, which is a sum of a negative (diamagnetic) contribution of the inner core electrons and a temperature independent paramagnetism, is positive, which is consistent with a small diamagnetic contribution of the present ligands[60], giving an opportunity for the temperature independent paramagnetism to prevail.

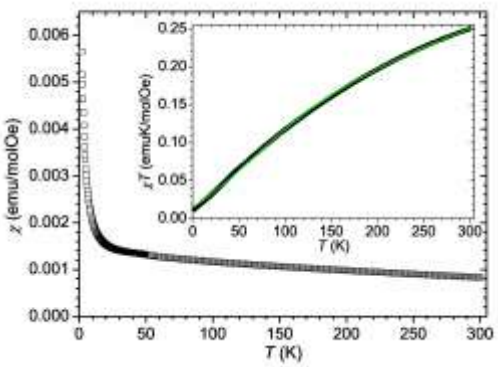

Fig. 5 Temperature dependent susceptibility χ and product χT (inset) of $V_4O_4(OH)_2(O_2CC_6H_4CO_2)_4\cdot$DMF and fit (full green line) to Eq. 1.

The combined structural and magnetic study in mutual interaction resulted with two kinds of oxidation states and coordination environments of vanadium cations: V^{4+} and V^{5+}, in equal amounts. The magnetic susceptibility shows that half of vanadium atoms carry a magnetic moment corresponding to spin 1/2 of V^{4+} ions, and another half is in non-magnetic state corresponding to V^{5+} ions. Modelling of magnetic results confirms that V^{4+} ions, on which magnetic moment is sitting, are arranged continuously in chains where the neighbours are interacting antiferromagnetically. In addition, the magnetic study gives also the exchange interaction between neighbouring V^{4+} ions of $J = -75$ K. Such a relatively strong interaction is usual for the oxygen bridges connecting the transition metal ions, present also here. Furthermore, V^{5+} ions are sitting on another chain-like substructure. Owing to diamagnetic state of V^{5+} it is possible to study the interaction in V^{4+} chain substructure. The presence of V^{5+} in V^{4+} chain would break the magnetic ordering, as there is no magnetic moment on V^{5+}. On the other hand, the presence of V^{4+} in V^{5+} chain would exhibit the large paramagnetic contribution. However, the observed small amount of paramagnetic centers of around $B = 3.8\%$, could be regarded as magnetic impurity originating from the surface, dislocations and other irregularities in the crystal leading to the broken structural and/or magnetic chains.

4 Conclusions

In summary, we have synthesized a new 2D layered nanocrystalline inorganic-organic hybrid, with the composition $V_4O_4(OH)_2(O_2CC_6H_4CO_2)_4 \cdot DMF$, using a simple solvothermal reaction between vanadium(V) oxytriisopropoxide with terephthalic acid in N,N-dimethylformamide. The crystal structure of this compound has been solved from the synchrotron X-ray powder diffraction pattern by combining a direct space method, and a constraint Rietveld refinement. The compound crystallizes in the monoclinic crystal system, in the space group P2/m (No. 10) with cell parameters: a = 20.923(4), b = 5.963(4), c = 20.425(1) Å, β = 123.70(6) º, V = 2120.1(9) Å^3, Z = 2. The crystal structure can be described as an array of parallel 2D layers running along [-101] direction, having vanadium in a mixed-valence state (+4 and +5 in equal proportion), and consequently consisting of two types of vanadium coordination polyhedra: face-shared trigonal prisms (V^{4+}) and distorted corner-shared square pyramids (V^{5+}). Both configurations form independent parallel chains oriented along the 2-fold symmetry crystallographic *b*-axis mutually interlinked with terephthalate ligand in a monodentate mode perpendicular to it. The whole structure has been stabilized by interlayer C–H···O hydrogen contacts via the structural N,N-dimethylformamide molecule. The morphology of as synthesized compound exhibits up to 10 microns long nanofibers, with the growth direction along a face diagonal of unit cell. The thermal analysis has revealed one-step decomposition attributed to the combustion of organic moieties and confirmed the proposed chemical formula deduced from an elemental analysis. Infrared absorption has evidenced constitutive molecular fragments, the small fraction of –COOH dimers and additionally corroborated a suggested a monodentate linking mode of organic moieties to the metal center. Finally, the magnetic susceptibility study showed that the magnetic properties of title compound can be described by linear antiferromagnetic chain model, with the isotropic exchange interaction of $J = -75$ K between the nearest V^{4+} neighbours of S = 1/2.

Acknowledgements

This work was funded by the Slovenian Research Agency (research programs P2-0145 and P2-030). I. D. thanks the Slovene Human Resources Development and Scholarship Fund „Ad Futura“ for supporting his research stay in Slovenia. We also acknowledge Dr. Radovan Černý for the synchrotron data collection, Edi Kranjc for the powder XRD recording, and Dajana Japič for IR spectrum acquisition.

Notes and references

[a] *Ruđer Bošković Institute, Bijenička 54, Zagreb, Croatia. Fax: +385 (0) 1 4680 114; Tel: +385 (0) 1 4561 111; E-mail: igor.djerdj@irb.hr*
[b] *National Institute of Chemistry, Hajdrihova 19, 1000 Ljubljana, Slovenia.*
[c] *Institute Jožef Stefan, Jamova 39, 1000 Ljubljana, Slovenia.*
[d] *Institute of Mathematics, Physics and Mechanics, Jadranska 19, 1000 Ljubljana, Slovenia.*
[e] *Faculty of Civil and Geodetic Engineering, University of Ljubljana, Jamova 2, 1000 Ljubljana, Slovenia.*
[f] *Department of Physics, Faculty of Science, University of Zagreb, Bijenička 32, 10000 Zagreb, Croatia.*
[g] *Faculty of Chemistry and Chemical Technology, University of Ljubljana, Aškerčeva 5, SI-1000 Ljubljana, Slovenia.*
[h] *Faculty of Computer and Information Science, University of Ljubljana, Tržaška cesta 25, SI-1000 Ljubljana, Slovenia.*

† Electronic Supplementary Information (ESI) available: Table S1 with refined structural parameters for non-H atoms of $V_4O_4(OH)_2(O_2CC_6H_4CO_2)_4 \cdot DMF$, and Figures S1-S2 with coordination environments of vanadium atoms. CCDC 818770 contains the supplementary crystallographic data for this paper. These data can be obtained free of charge from The Cambridge Crystallographic Data Centre via www.ccdc.cam.ac.uk/data_request/cif. See DOI: 10.1039/b000000x/

1. G. Ferey, *Chem. Mater.*, 2001, **13**, 3084-3098.
2. D. Hagrman, P. J. Hagrman and J. Zubieta, *Angew. Chem. Int. Ed.*, 1999, **38**, 3165-3168.
3. J. C. Tan and A. K. Cheetham, *Chem. Soc. Rev.*, 2011, **40**, 1059-1080.
4. M. Kosa, J. C. Tan, C. A. Merrill, M. Krack, A. K. Cheetham and M. Parrinello, *ChemPhysChem*, 2010, **11**, 2332-2336.
5. P. J. Hagrman, D. Hagrman and J. Zubieta, *Angew. Chem. Int. Ed.*, 1999, **38**, 2639-2684.
6. P. Y. Feng, X. H. Bu and N. F. Zheng, *Acc. Chem. Res.*, 2005, **38**, 293-303.
7. G. Ferey, C. Mellot-Draznieks, C. Serre and F. Millange, *Acc. Chem. Res.*, 2005, **38**, 217-225.
8. X. J. Gu, Z. H. Lu, H. L. Jiang, T. Akita and Q. Xu, *J. Am. Chem. Soc.*, 2011, **133**, 11822-11825.
9. C. Montoro, F. Linares, E. Q. Procopio, I. Senkovska, S. Kaskel, S. Galli, N. Masciocchi, E. Barea and J. A. R. Navarro, *J. Am. Chem. Soc.*, 2011, **133**, 11888-11891.
10. M. Eddaoudi, J. Kim, N. Rosi, D. Vodak, J. Wachter, M. O'Keeffe and O. M. Yaghi, *Science*, 2002, **295**, 469-472.
11. M. J. Kim, S. M. Park, S. J. Song, J. Won, J. Y. Lee, M. Yoon, K. Kim and G. Seo, *J. Colloid Interface Sci.*, 2011, **361**, 612-617.
12. I. Djerdj, M. H. Cao, X. Rocquefelte, R. Cerny, Z. Jaglicic, D. Arcon, A. Potocnik, F. Gozzo and M. Niederberger, *Chem. Mater.*, 2009, **21**, 3356-3369.
13. M. Riou-Cavellec, D. Riou and G. Ferey, *Inorg. Chim. Acta*, 1999, **291**, 317-325.
14. P. J. Saines, H. H. M. Yeung, J. R. Hester, A. R. Lennie and A. K. Cheetham, *Dalton Trans.*, 2011, **40**, 6401-6410.

15. A. K. Cheetham, G. Ferey and T. Loiseau, *Angew. Chem. Int. Ed.*, 1999, **38**, 3268-3292.
16. M. H. Cao, I. Djerdj, Z. Jaglicic, M. Antonietti and M. Niederberger, *Phys. Chem. Chem. Phys.*, 2009, **11**, 6166-6172.
17. Q. Ye, Y.-M. Song, G.-X. Wang, K. Chen, D.-W. Fu, P. W. Hong Chan, J.-S. Zhu, S. D. Huang and R.-G. Xiong, *J. Am. Chem. Soc.*, 2006, **128**, 6554-6555.
18. C. N. R. Rao, A. K. Cheetham and A. Thirumurugan, *J. Phys.: Condens. Matter*, 2008, **20**, 083202.
19. A. Stroppa, P. Jain, P. Barone, M. Marsman, J. M. Perez-Mato, A. K. Cheetham, H. W. Kroto and S. Picozzi, *Angew. Chem. Int. Ed.*, 2011, **50**, 5847-5850.
20. P. Jain, V. Ramachandran, R. J. Clark, H. D. Zhou, B. H. Toby, N. S. Dalal, H. W. Kroto and A. K. Cheetham, *J. Am. Chem. Soc.*, 2009, **131**, 13625-13627.
21. Z. C. Orel, M. Gaberscek and A. Turkovic, *Sol. Energy Mater. Sol. Cells*, 2005, **86**, 19-32.
22. I. Djerdj, D. Sheptyakov, F. Gozzo, D. Arcon, R. Nesper and M. Niederberger, *J. Am. Chem. Soc.*, 2008, **130**, 11364-11375.
23. P. Kanoo, A. C. Ghosh and T. K. Maji, *Inorg. Chem.*, 2011, **50**, 5145-5152.
24. N. A. Khan, J. W. Jun, J. H. Jeong and S. H. Jhung, *Chem. Commun.*, 2011, **47**, 1306-1308.
25. K. Barthelet, J. Marrot, D. Riou and G. Ferey, *Angew. Chem. Int. Ed.*, 2002, **41**, 281-284.
26. K. Barthelet, D. Riou and G. Ferey, *Chem. Commun.*, 2002, 1492-1493.
27. J. M. Breen and W. Schmitt, *Angew. Chem. Int. Ed.*, 2008, **47**, 6904-6908.
28. C. Allain, S. Favette, L. M. Chamoreau, J. Vaissermann, L. Ruhlmann and B. Hasenknopf, *Eur. J. Inorg. Chem.*, 2008, 3433-3441.
29. S. Cevik, M. Poyraz, M. Sari and O. Buyukgungor, *J. Chem. Cryst.*, 2007, **37**, 497-502.
30. X. M. Zhang, J. J. Hou, W. X. Zhang and X. M. Chen, *Inorg. Chem.*, 2006, **45**, 8120-8125.
31. F. A. A. Paz, Y. Z. Khimyak, A. D. Bond, J. Rocha and J. Klinowski, *Eur. J. Inorg. Chem.*, 2002, 2823-2828.
32. L. Pan, N. Ching, X. Y. Huang and J. Li, *Inorg. Chem.*, 2000, **39**, 5333-5340.
33. L. S. Long, Y. P. Ren, L. H. Ma, Y. B. Jiang, R. B. Huang and L. S. Zheng, *Inorg. Chem. Commun.*, 2003, **6**, 690-693.
34. D. Y. Hong, Y. K. Hwang, C. Serre, G. Ferey and J. S. Chang, *Adv. Funct. Mater*, 2009, **19**, 1537-1552.
35. G. X. Liu, K. Zhu, H. M. Xu, S. Nishihara, R. Y. Huang and X. M. Ren, *Crystengcomm*, 2009, **11**, 2784-2796.
36. K. Barthelet, J. Marrot, G. Ferey and D. Riou, *Chem. Commun.*, 2004, 520-521.
37. X. M. Lin, H. C. Fang, Z. Y. Zhou, L. Chen, J. W. Zhao, S. Z. Zhu and Y. P. Cai, *Crystengcomm*, 2009, **11**, 847-854.
38. N. L. Rosi, M. Eddaoudi, J. Kim, M. O'Keeffe and O. M. Yaghi, *Angew. Chem. Int. Ed.*, 2002, **41**, 284-287.
39. Z. Y. Fu, X. T. Wu, J. C. Dai, S. M. Hu and W. X. Du, *New J. Chem.*, 2002, **26**, 978-980.
40. A. Thirumurugan and A. K. Cheetham, *Eur. J. Inorg. Chem.*, 2010, 3823-3828.
41. Z. Hulvey, J. D. Furman, S. A. Turner, M. Tang and A. K. Cheetham, *Cryst. Growth Des.*, 2010, **10**, 2041-2043.
42. M. Niederberger, *Acc. Chem. Res.*, 2007, **40**, 793-800.
43. N. Pinna and M. Niederberger, *Angew. Chem. Int. Ed.*, 2008, **47**, 5292-5304.
44. P. H. Mutin and A. Vioux, *Chem. Mater.*, 2009, **21**, 582–596.
45. N. Pinna, G. Garnweitner, P. Beato, M. Niederberger and M. Antonietti, *Small*, 2005, **1**, 112-121.
46. I. Olliges-Stadler, M. D. Rossell and M. Niederberger, *Small*, 2010, **6**, 960-966.
47. I. Djerdj, G. Garnweitner, D. S. Su and M. Niederberger, *J. Solid State Chem.*, 2007, **180**, 2154-2165.
48. I. Djerdj, D. Arcon, Z. Jaglicic and M. Niederberger, *J. Solid State Chem.*, 2008, **181**, 1571-1581.
49. I. Djerdj, G. Garnweitner, D. Arcon, M. Pregelj, Z. Jaglicic and M. Niederberger, *J. Mater. Chem.*, 2008, **18**, 5208-5217.
50. A. Boultif and D. Louer, *J. Appl. Cryst.*, 2004, **37**, 724-731.
51. V. Favre-Nicolin and R. Černý, *J. Appl. Cryst.*, 2002, **35**, 734-743.
52. J. Rodriguez-Carvajal, Laboratorie Leon Brillouin, CEA-Saclay, France, July 2001 edn., 2001.
53. O. V. Dolomanov, L. J. Bourhis, R. J. Gildea, J. A. K. Howard and H. Puschmann, *J. Appl. Cryst.* , 2009, **42**, 339-341.
54. L. Sacconi, *Pure Appl. Chem.*, 1968, **17**, 95-128.
55. I. D. Brown and W. Kang Kun, *Acta Cryst.*, 1976, **B32**, 1957-1959.
56. A. Tocchetto and A. Glisenti, *Langmuir*, 2000, **16**, 6173-6182.
57. M. Caravati, J.-D. Grunwaldt and A. Baiker, *Phys. Chem. Chem. Phys.*, 2005, **7**, 278-285.
58. W. E. Estes, D. P. Gavel, W. E. Hatfield and D. J. Hodgson, *Inorg. Chem.*, 1978, **17**, 1415-1421.
59. J. C. Bonner and M. E. Fisher, *Phys. Rev.* , 1964, **135**, A640-A658.
60. O. Kahn, *Molecular Magnetism*, VCH Publishers, 1993.

Igor Djerdj,* Srečo D. Škapin, Miran Čeh, Zvonko Jagličić, Damir Pajić, Bojan Kozlevčar, Bojan Orel, and Zorica Crnjak Orel

Interplay between the Structural and Magnetic Probes in Elucidation of the Structure of Novel 2D Layered $V_4O_4(OH)_2(O_2CC_6H_4CO_2)_4 \cdot DMF$

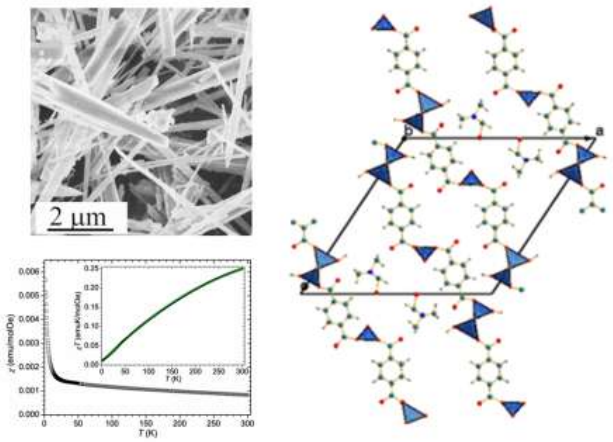

Interplay between the structural and magnetic probes is crucial in the elucidation of the geometric structure of novel 2D layered fiber-like coordination polymer.